(A)geostrophic adjustment of dipolar perturbations, formation of coherent structures and their properties, as follows from high-resolution numerical simulations with rotating shallow water model

Bruno Ribstein, Jonathan Gula, Vladimir Zeitlin

(A)geostrophic adjustment of dipolar perturbations, formation of coherent structures and their properties, as follows from high-resolution numerical simulations with rotating shallow water model

Bruno Ribstein, Jonathan Gula, and Vladimir Zeitlin

Citation: Physics of Fluids (1994-present) **22**, 116603 (2010); doi: 10.1063/1.3514200
View online: http://dx.doi.org/10.1063/1.3514200
View Table of Contents: http://scitation.aip.org/content/aip/journal/pof2/22/11?ver=pdfcov
Published by the AIP Publishing

(A)geostrophic adjustment of dipolar perturbations, formation of coherent structures and their properties, as follows from high-resolution numerical simulations with rotating shallow water model

Bruno Ribstein, Jonathan Gula, and Vladimir Zeitlin[a)]
LMD, ENS, and Univ. P. and M. Curie, 24 rue Lhomond, Paris 75005, France

(Received 1 July 2010; accepted 8 October 2010; published online 11 November 2010)

In the general context of the geostrophic adjustment, we study the formation of coherent structures in a rotating shallow water model on the *f*-plane starting from localized dipolar configurations. We perform direct numerical simulations with such initial conditions with the help of a well-balanced high-resolution finite-volume numerical scheme. Initializations with geostrophically balanced quasigeostrophic modons with high enough Rossby numbers lead to adjustment toward quasistationary coherent ageostrophic dipoles. Like in laboratory experiments, cyclonic potential vorticity is being detrained from the dipoles and their trajectories bend. Comparisons with recently found exact steady-moving localized dipolar solutions show similarities and differences at the same time. Initializations with unbalanced dipolar initial conditions lead to similar quasistationary configurations at high enough effective Rossby numbers. At low Rossby numbers the classical geostrophic adjustment is observed. Ageostrophic quasistationary dipoles emerging from the simulations are surprisingly robust. They undergo frontal collisions with an exchange of cyclonic partners, which are essentially elastic and do not change their structure. They also keep coherence when encountering a steep topography and ballistically transport passive tracers. © *2010 American Institute of Physics*. [doi:10.1063/1.3514200]

I. INTRODUCTION

Geostrophic adjustment which consists in relaxation, by emission of inertia-gravity waves, of any perturbation in a rotating stratified fluid toward a state of geostrophic equilibrium, i.e., the equilibrium between the pressure and the Coriolis forces, is a universal process, see, e.g., Ref. 1. Fluid motions close to the geostrophic equilibrium are governed by the so-called balanced, slow dynamics. The simplest and best-known balanced model is the quasigeostrophic (QG) one, see, e.g., Ref. 2. If variations of the Coriolis parameter are neglected (which corresponds to the *f*-plane approximation in geophysical fluid dynamics), the QG-model is essentially equivalent to the two-dimensional (2D) Euler equations (in the absence of dissipation) in vorticity-streamfunction variables related via Laplace (in the case of infinite deformation radius) or Helmholtz (in the case of finite deformation radius) operators.

The universality of the geostrophic adjustment of localized initial perturbations and the validity of the balanced dynamics can be established analytically in the limit of fast rotation, i.e., small Rossby numbers, by the method of multiscale asymptotic expansions in a series of models,[3,4] in particular within the framework of rotating shallow water model (RSW), which is a standard conceptual model in geophysical fluid dynamics.

Although the limit of small Rossby number (Ro) is relevant for large-scale atmospheric and oceanic motions,[2] a general question arises how the scenario of the geostrophic adjustment is modified with increasing Rossby numbers. A way to study such modifications is to take as initial condition in a full RSW model a solution of the QG equations and follow its evolution. While no or small departures from this solution are expected at small enough Ro, they would probably appear at large enough Ro. Due to its proximity to 2D Euler equations, the QG model possesses exact solutions in a form of localized multipolar vortices. Monopolar steady vortices being rather trivial, we will concentrate on steadily moving dipolar vortices, the modons, which are the QG analogs of Chaplygin–Lamb's dipole solution of 2D Euler equations.[5] The question, therefore, is how far a QG modon perturbation will depart from its initial form in RSW simulations or, more generally, how close to these solutions will stay initial dipolar perturbations in RSW during their evolution. An additional motivation for such study is provided by recent results by Kizner *et al.*,[6] who demonstrated the existence of steady propagating exact *ageostrophic* modon solutions of the full RSW equations on the *f*-plane. Will these solutions, rather than QG modons, result from the adjustment process at high enough Ro? Beyond the adjustment context, the answer to this question would allow to have an idea of the domain of attraction of newly found solutions.

Below we report the results of direct numerical simulations (DNSs) of the adjustment of dipolar configurations which were accomplished with new-generation high-resolution finite-volume numerical scheme for RSW equations.[7] It is:

(1) Weakly dissipative, with numerical dissipation concentrated in the high-gradient zones (shocks) and the energy necessarily decreasing across shocks, if any (the "entropy" property);

[a)]Electronic mail: zeitlin@lmd.ens.fr.

(2) Well balanced, i.e., preserves geostrophic equilibria, and conserves well the potential vorticity in the absence of shocks;
(3) Allows a variety of boundary conditions, periodic, free-slip, sponges, and handles well flows over topography.

It was exhaustively tested in a number of applications, e.g., Refs. 8 and 9.

We show that, although at low enough Ro the adjustment of dipolar structures is, indeed, geostrophic and results in QG modons, it becomes *ageostrophic* with increasing Ro and, at least for certain classes of initial conditions, produces long-living coherent dipolar vortices with significant deviations from the geostrophic balance. Although these vortices have much in common with the "ageostrophic modons" of Ref. 6, they are still different. Apart from differences in profiles of height, velocity, and potential vorticity, mainly in the anticyclonic part of the dipole, a qualitative difference consists in curved trajectory and persisting detrainment of (weak) cyclonic potential vorticity, like for dipoles in the rotating fluid experiments.[10] Moreover, we show that modons of Ref. 6 themselves, taken as initial conditions, undergo adjustment which modifies their structure. We provide detailed diagnostics of the adjustment process and of the resulting coherent structures and illustrate some of their properties.

The paper is organized as follows: in Sec. II we present results of the adjustment process for different initial dipolar configurations, both balanced (QG modon) and unbalanced (velocity or pressure perturbations alone). We mostly concentrate on the "ageostrophic adjustment" of the QG modons at high enough Ro, the formation of coherent structures and their characteristics. In Sec. III we sketch the transport properties of the ageostrophic modons and illustrate their mutual interactions and interactions with topography. In Sec. IV we present simulations initialized with the solutions of Ref. 6 and comparisons with previous calculations. Section V contains summary and discussion.

II. ADJUSTMENT OF DIPOLAR INITIAL PERTURBATIONS IN RSW ON THE *f*-PLANE AS FOLLOWS FROM DNS

A. RSW and QG equations and the QG modon solution: A reminder

The RSW equations on the f-plane read

$$(\partial_t + u\partial_x + v\partial_y)u - fv + g'\partial_x H = 0,$$
$$(\partial_t + u\partial_x + v\partial_y)v + fu + g'\partial_y H = 0, \tag{2.1}$$
$$\partial_t H + \partial_x(Hu) + \partial_y(Hv) = 0.$$

Here u and v are the x- and y-components of the velocity, H is the thickness of the shallow water layer, H_0 is its unperturbed value, f=const. is the Coriolis parameter, and g' is the reduced gravity. It is useful to keep in mind that the RSW equations are equivalent to two-dimensional barotropic gas dynamics in the presence of the Coriolis force. The characteristic inertia-gravity waves (IGWs) of the RSW model are equivalent to sound waves in the presence of rotation.

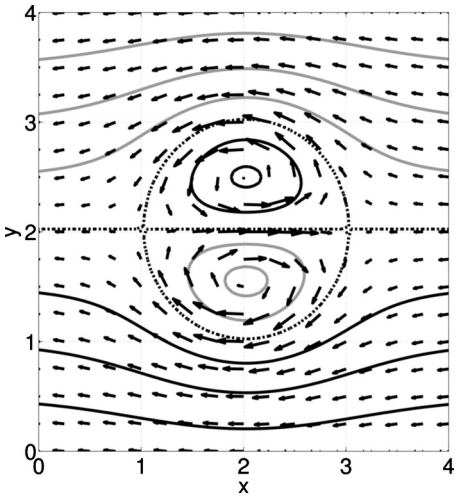

FIG. 1. Isolines of the comoving streamfunction $\Psi=h+y$ and the velocity field $(u-U,v-V)$ (arrows) for the QG modon at Ro=0.2. $\Psi>0$: black. $\Psi<0$: gray. Dashed line: the separatrix delimiting the inner region of recirculating fluid. Contour interval 0.1.

The potential vorticity (PV)

$$q = \frac{\partial_x v - \partial_y u + f}{H},$$

and its anomaly $Q=q-f/H_0$ are Lagrangian invariants. For steadily moving solutions of Eq. (2.1), another useful quantity is the Bernoulli function B, calculated in a frame of reference moving with the velocity $(\bar{U},\bar{V})$,

$$B = \tfrac{1}{2}(u-\bar{U})^2 + \tfrac{1}{2}(v-\bar{V})^2 + g'H + \bar{U}fy - \bar{V}fx.$$

The Bernoulli function and the PV are functionally related[11] for a steadily moving solution of Eq. (2.1).

For fluid motions close to geostrophic balance in the limit of small Rossby numbers $\mathrm{Ro}=U/fL\to 0$, where U and L are typical velocity and spatial scales, the approximate QG equation follows (in nondimensional form):

$$\partial_T(\nabla^2 h - \Lambda^2 h) + \mathcal{J}(h,\nabla^2 h) = 0. \tag{2.2}$$

Here the height perturbation $h=H-H_0$ plays the role of streamfunction via the geostrophic wind relations, $\Lambda^2=L^2/L_R^2$ is the inverse Burger number which should be of the order unity to guarantee the validity of Eq. (2.2), $L_R=\sqrt{g'H_0}/f$ is the deformation radius, and T is the slow time measured in Ro f^{-1} units. It is clear from Eq. (2.2) that IGWs are filtered out in this approximation.

The geostrophic modon is an exact localized dipolar vortex solution of Eq. (2.2) generalizing the Chaplygin–Lamb vortex solution of 2D Euler equations (see, e.g., Ref. 12) to finite deformation radius. It was first written down in Ref. 5. The geostrophic modon travels steadily without change of form at a constant speed U, e.g., along the x-axis. Because of steady translation, the variables u, v, and h are functions of $x-Ut$ and y only. The explicit form of the nondimensional comoving geostrophic modon streamfuncion $\Psi=h+y$ in polar coordinates (r,θ) associated with $(x-Ut,y)$ is

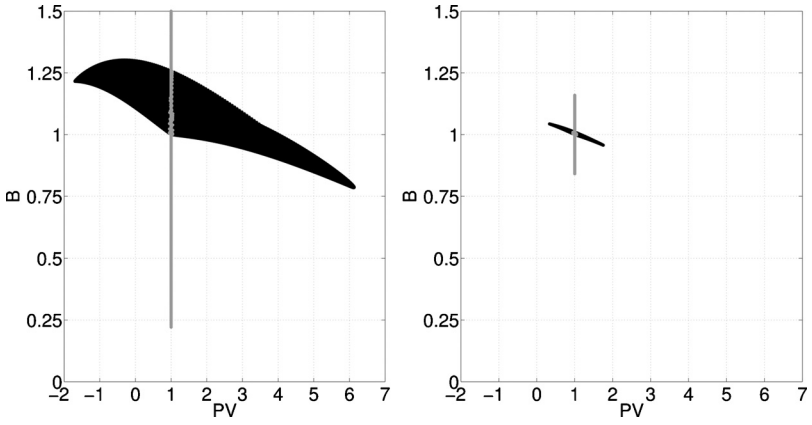

FIG. 2. Scatter plots of the Bernoulli function vs PV for QG modon at Ro=0.2 (left panel) and Ro=0.04 (right panel). Black: inner region (inside the separatrix). Gray: outer region.

$$\Psi = \left[\frac{J_1(\Pi r/L)}{J_1(\Pi)} - \frac{r}{L}\right]\left(\frac{\Lambda}{\Pi}\right)^2 \sin\theta \quad r < L,$$
$$= \left[\frac{r}{L} - \frac{K_1(\Lambda r/L)}{K_1(\Lambda)}\right]\sin\theta \quad r \geq L. \tag{2.3}$$

Here J_1 and K_1 are the first order Bessel and modified Bessel functions and $\Pi = \sqrt{A^2 - \Lambda^2}$ with A=const. For this solution, the nondimensional anomaly of quasigeostrophic potential vorticity $Q_G = \nabla^2 h - \Lambda^2 h$ is zero outside a circular separatrix of radius L and proportional to Ψ inside, with a proportionality constant—A^2. The velocity anomaly $(u-U, v-V)$ and comoving streamfunction distributions for this solution are presented in Fig. 1. Its characteristic feature is perfect cyclone—anticyclone symmetry. However, Eq. (2.3) is not a solution of full RSW Eq. (2.1), as shown in Fig. 2, where the scatter plots of the Bernoulli function versus PV calculated for the QG modon in RSW are shown for small and large Ro. Let us remind, see Ref. 6, that such scatter plots should give a line for exact solutions.

Starting from Eq. (2.3), exact *ageostrophic modon* solutions of Eq. (2.1) having a pronounced cyclone-anticyclone asymmetry were constructed in Ref. 6 by iterations in the RSW equations restricted to configurations steady moving along the straight paths. Nothing is known about their stability yet.

B. Adjustment of QG modons and formation of ageostrophic coherent structures

We present the results of numerical simulations of the adjustment of dipolar configurations in the RSW model starting from the most striking case of "ageostrophic adjustment" of initially balanced initial conditions for the velocity and the layer thickness corresponding to a QG modon with $\Lambda=1$; Ro=0.2. Figure 3 shows the evolution of the thickness anomaly. Only a portion of the computational domain is shown in the figures which follow, the full domain being $40L_R \times 40L_R$. The spatial resolution of the simulations presented below is $dx = dy = 0.05L_R$. Hereafter time is nondimensionalized by f^{-1}, length by L_R, height by H_0, and acceleration by g'. In all simulations of this section we used periodic boundary conditions, which are energetically neutral. The flow rapidly (in a couple of inertial periods) adjusts to a quasistationary ageostrophic dipolar configuration by emitting IGW, clearly seen in the middle panel of Fig. 3, as well as in the left panel of Fig. 6 below. An important reorganization of the dipole takes place during adjustment, as follows from Fig. 4, where the corresponding evolution of the PV is presented. As seen in the figure, the initial cyclone-anticyclone symmetry is being destroyed during adjustment, which is confirmed by the comparison of thickness and velocity fields at $t=0$ and $t=100$ presented in Fig. 5. The ageo-

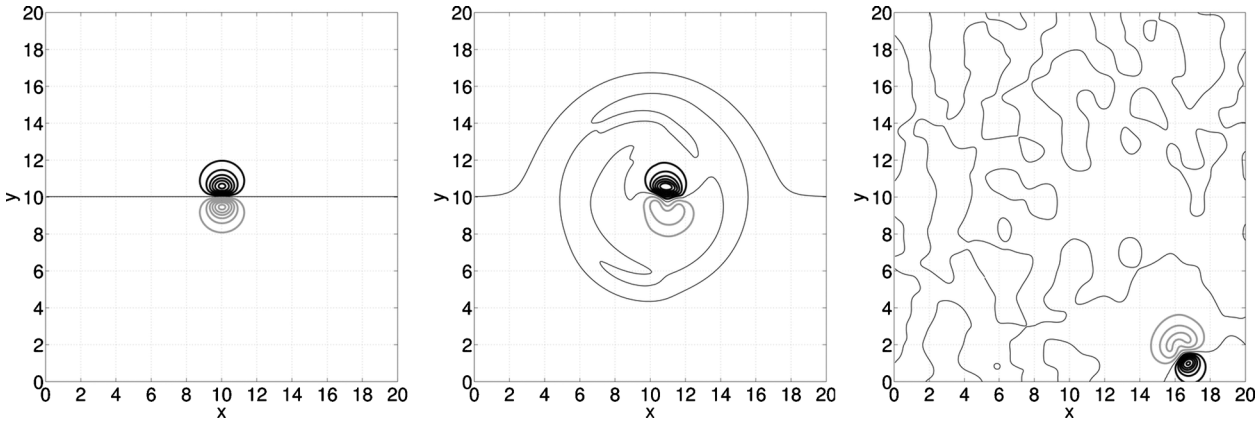

FIG. 3. Adjustment of the initial QG modon configuration with Ro=0.2, as seen in the thickness field. $t=0$, 10, and 100, from left to right. Thin line: the line of zero thickness anomaly. Black: cyclone. Gray: anticyclone. Contour interval: 0.05, the thickness anomaly taking values in the interval $[-0.4;0.3]$ during the simulation.

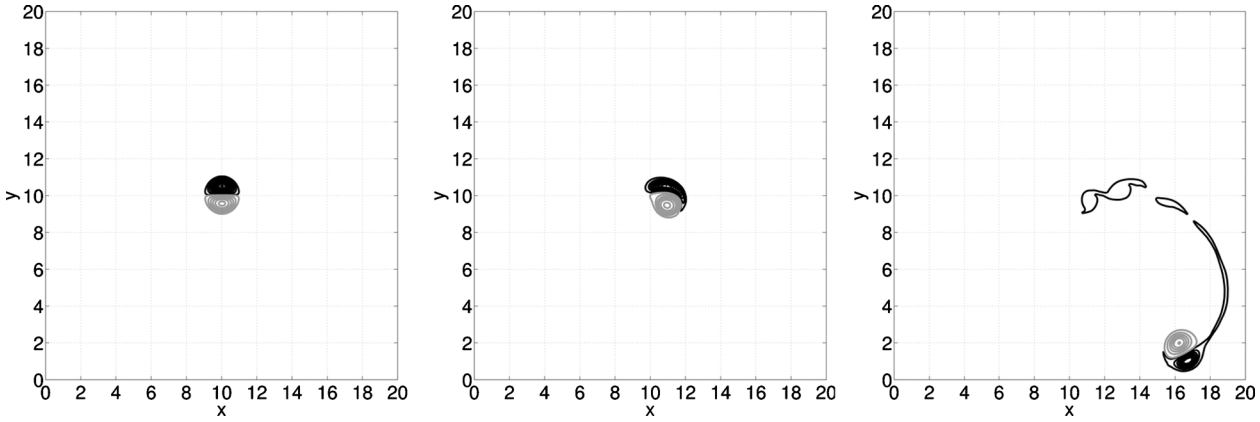

FIG. 4. Adjustment of the initial QG modon configuration with Ro=0.2, as seen in the PV field. $t=0$, 10, and 100, from left to right. Black: cyclone. Gray: anticyclone. Contour interval: 0.5, the lowest value of the full PV anomaly $|Q|=0.05$, PV anomaly taking values in the interval $[-2.7;5.1]$ during the simulation.

strophic character of the "adjusted" state with the velocity field not following the isobars is obvious from the figure. Geostrophic adjustment of the initial configuration which is already in geostrophic balance may seem paradoxical. However, the Rossby number of the initial configuration is high enough and ageostrophic effects are thus important from the beginning. It is worth emphasizing that our definition of the Rossby number is global. The local Rossby number defined as the ratio of the local relative to planetary vorticity goes up to 3.2 in this configuration. The system, thus, is driven toward a new quasistationary state which is manifestly not in geostrophic balance.

An indicator of ageostrophy is the divergence of the velocity field, the balanced geostrophic velocity being, obviously, divergenceless. The evolution of the divergence field in the simulation of Figs. 3 and 4 is presented in Fig. 6. One clearly sees on the left panel the IGW which, unlike the balanced vortices, do have divergence signature. This comforts our interpretation of the initial stage of the adjustment process. Note a distinctive quadrupolar structure of the divergence field which is centered at the cyclonic part of the dipole. This confirms, again, an ageostrophic character of the adjusted vortex. Integrating the modulus of the divergence of the velocity field over a domain of the flow containing the dipole

$$D = \int dxdy|\partial_x u + \partial_y v|, \tag{2.4}$$

one obtains a quantitative measure of ageostrophic motions. In what follows the integration domain is chosen to be a circle of radius $3L_R$ centered at the modon, which corresponds roughly to the modon boundary as seen in the thickness anomaly and velocity field, see Fig. 5 (note that PV distribution of the modon is much more compact, see Fig. 4). The measure D may be compared with the modulus of the vorticity integrated over the same domain which has the same dimensions, or integrated positive or negative vorticity anomalies (cyclonic and anticyclonic circulations, respectively), having contributions mostly from the balanced vortical motions,[13]

$$\Gamma_{\pm} = \int dxdy(\partial_x v - \partial_y u)_{\pm}. \tag{2.5}$$

With the above-described scaling the values of these quantities at, e.g., $t=50$, are $D \approx 0.34$, $\Gamma_+ \approx 2.05$, and $\Gamma_- \approx 2.15$, which shows that the intensity of ageostrophic motions is $\mathcal{O}(\mathrm{Ro})$ less than typical circulation. Recall that divergence of the initial QG modon is identically zero. It jumps due to the initial adjustment and then gradually diminishes at approxi-

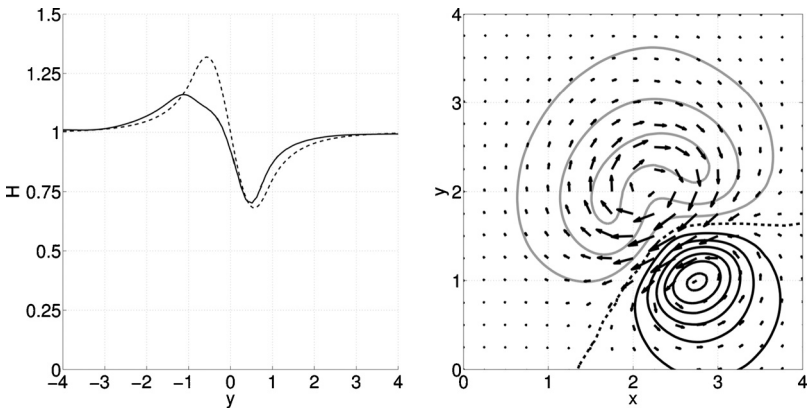

FIG. 5. Comparison of the thickness anomaly at $t=0$ (dotted) and $t=100$ (solid) states (left panel), and thickness (contour) and velocity (arrows) distributions of the final state (right panel). Black: cyclone. Gray: anticyclone. Contour interval: 0.05.

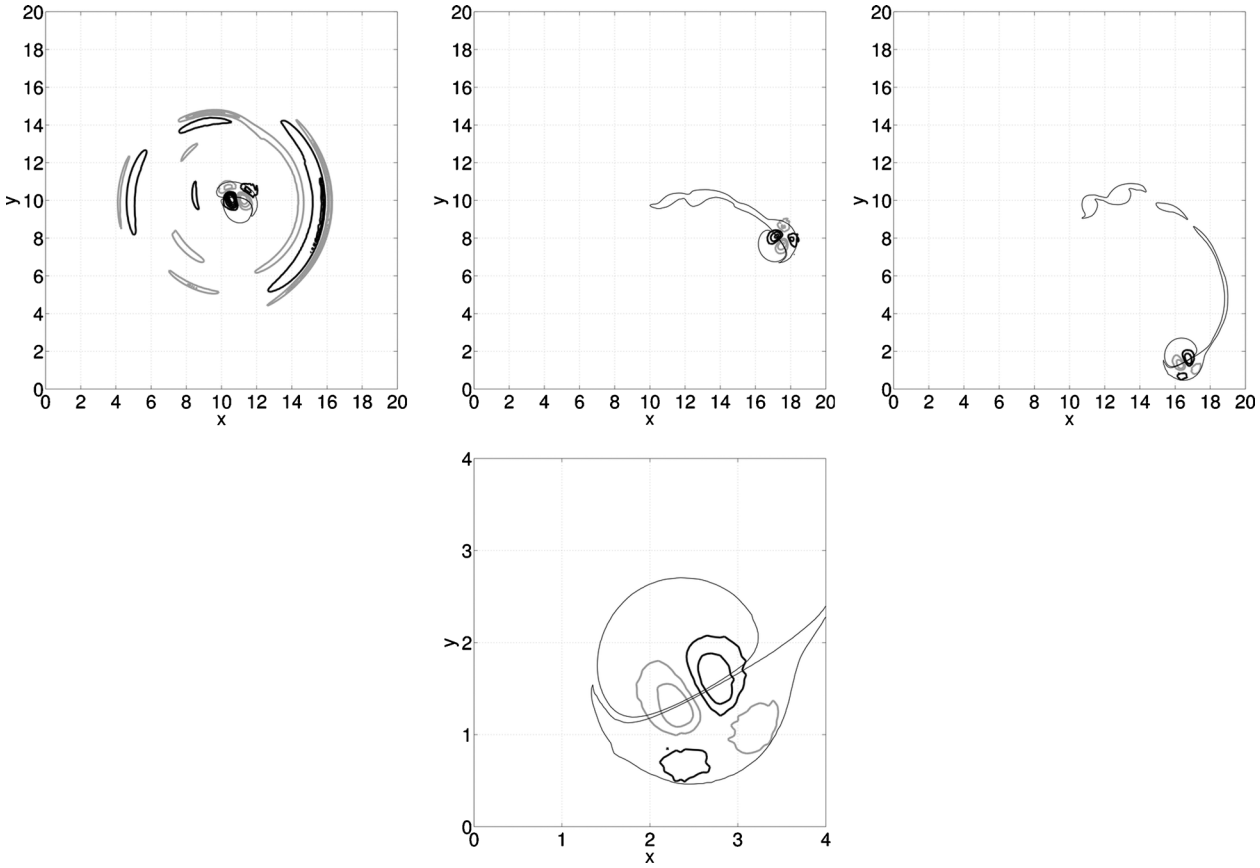

FIG. 6. Adjustment of the initial QG modon configuration with Ro=0.2, as seen in the divergence field. t=5, 45, and 100, from left to right, and a zoom of the dipole at t=100 in the lower panel. Contours with small PV anomaly $|Q|$=0.05 are superimposed (thin lines) for the sake of comparison with Fig. 4. Black: divergence. Gray: convergence. Contour interval: 0.05, the divergence field taking values in the interval [−0.2;0.3] during the simulation.

mately the same rate as anticyclonic circulation in Fig. 7 below (not shown). It is worth noting in this context that if for the same simulation we calculate the QG ageostrophic velocity from the tendency of the geostrophic relative vorticity, according to the standard rules (e.g., Ref. 3), we get the value $\mathcal{O}(\mathrm{Ro}^2)$.

The propagation speed of the ageostrophic modon is lower than of the geostrophic one (in the experiment of Fig. 3, $|U|_{AG}\approx.15$, and U_G=.2), while the modon trajectory is curved, see Fig. 4. The estimated rate of trajectory bending, which may be interpreted as an instability of a straight-moving structure, is 0.07–0.09 at the initial stage of evolution.[14]

Weak cyclonic PV (with values of Q typically less than 0.05) is continuously detrained from the vortex along the separatrix in the form of vortex filaments, which are eventually cut off due to nonzero, albeit small, numerical diffusivity. The bending of the modon trajectory is due to the difference in circulations of the vortices which develops during the evolution of the dipole as follows from Fig. 7, where a comparative evolution of cyclonic and anticyclonic circulations in the dipole is displayed. In this and subsequent simulations, the cyclonic (anticyclonic) component of the dipole is defined as a simply connected domain inside the contour corresponding to the PV anomaly value of +(−)0.05 and the modon as a whole is defined as the union of these two contours. This definition is maintained throughout the paper. The circulation is defined as an integral of relative vorticity over the component area, see Eq. (2.5). Sharp drops in cyclonic circulation at $t\approx80$ and $t\approx100$ correspond to detachment of vortex filaments (see Fig. 4, right panel) when, respectively, about 10% and about 3% of the circulation of the cyclonic partner of the dipole are gone.

It is easy to understand, e.g., from the point-vortex analogy, that the trajectory of the dipole is bended toward the

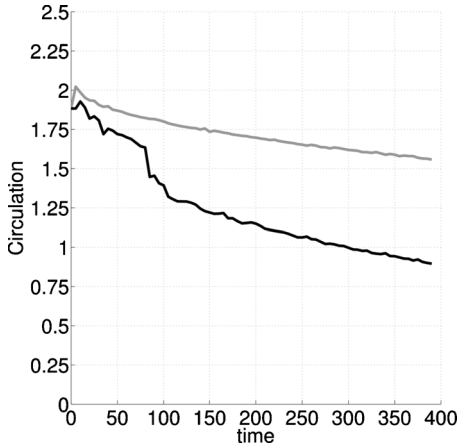

FIG. 7. Evolution of cyclonic (black) and anticyclonic (gray) circulations in the dipole. Sharp drops in cyclonic circulation at $t\approx80$ and $t\approx100$ correspond to detachment of vortex filaments, see Fig. 4, right panel.

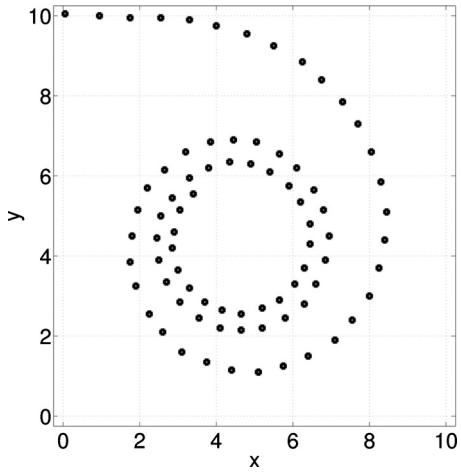

FIG. 8. Modon position at time intervals 5 up to $t=400$.

stronger vortex. As follows from the figure, the cyclonic circulation decreases faster, the imbalance between cyclonic and anticyclonic components of the dipole grows, and the curvature of the trajectory should increase in time. Long-time simulations show that the trajectory of the ageostrophic modon is, in fact, a spiral, as shown in Fig. 8.

In spite of the above-described slow changes, the adjusted dipole is indeed a coherent structure, as follows from the evolution of the scatter plot toward lesser dispersion, see Fig. 9. Let us remind that for steady solutions of the RSW equations with rectilinear propagation both Bernoulli function and PV are some functions of the streamfunction (see, Refs. 6 and 11), and hence should give a line in the B-PV plane. The PV in the outer with respect to the vortex region is uniform, apart from the debris of cut-off filaments with very weak PV anomaly, and equal to one in our scaling. The black admixture to the gray line in the right panel of Fig. 9 originates from the uncut filament, see Fig. 4, with almost zero PV anomaly.

The energetics of the dipole and of its cyclonic and anticyclonic components is presented in Fig. 10, where we show the evolution of the nonnormalized total energy, as well as its kinetic and available potential energy components, and also the evolution of the energies of cyclonic and anticyclonic components. We see that after an abrupt initial energy loss related to IGW emission, the energy of the dipole decreases quasimonotonically due to numerical dissipation. This should be compared to the evolution of the total energy in the computational domain presented in Fig. 11. Although a significant portion of energy is lost at the end of the simulation due to numerical dissipation, it should not be forgotten that our runs lasted more than 400 inertial periods.

As follows from Fig. 10, the dissipation is not symmetric, the cyclonic component losing more energy. This is consistent with the fact that the gradients of thickness and velocity fields are higher there, see Fig. 5. The detrainement and cut-off of the cyclonic PV (see Fig. 4) may also play a role. This latter may be explained by weak numerical diffusion, which has the most pronounced effect in the vicinity of the saddle point in the comoving frame, where the trajectories of fluid particles are notoriously unstable, and subsequent entrainment by the ambient flow. However, the estimates show that the role of filaments in energetics is rather negligible. Indeed, the total energy decrease rates in Figs. 10 and 11 are practically identical, although it is only the first which is affected by the cut-off of the filaments. Direct calculation of the energy of the filament on the right panel of Fig. 4 right after its detachments gives that its kinetic energy is about 0.02% and its available potential energy is about 0.2%, as compared to the cyclonic partner of the dipole.

It should be stressed that the bending trajectory and detrainment of the weak cyclonic PV are very similar to that observed for dipoles in the rotating fluid experiments and in corresponding simulations with asymmetric Ekman friction.[10] Numerical dissipation in our code (note that no explicit dissipation is introduced) acts in the present simulation more vigorously on the higher-gradient cyclones, with the same effect.

Let us finally emphasize that the ageostrophic phenomena observed in the displayed simulation are attenuated with decreasing Rossby number of the initial QG modon. Indeed, at small Ro the QG modons resemble more the steady solutions of the RSW equations, as follows from the right panel of Fig. 2. Therefore, they are less and less subject to ageo-

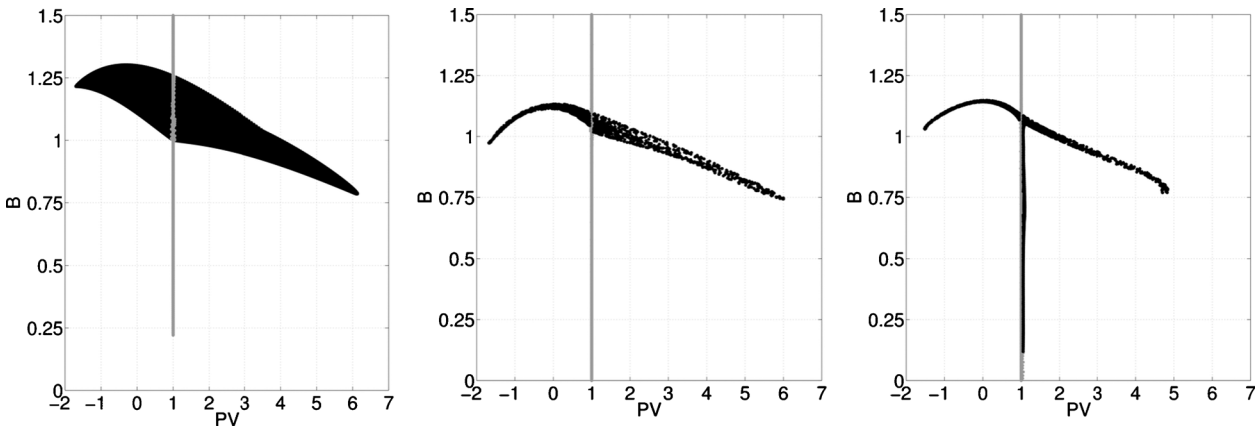

FIG. 9. Adjustment of the initial QG modon configuration with Ro=0.2, as seen in the scatter plot of Bernoulli function vs PV. $t=0$, 5, and 100, from left to right. Black: modon core. Gray: outer region.

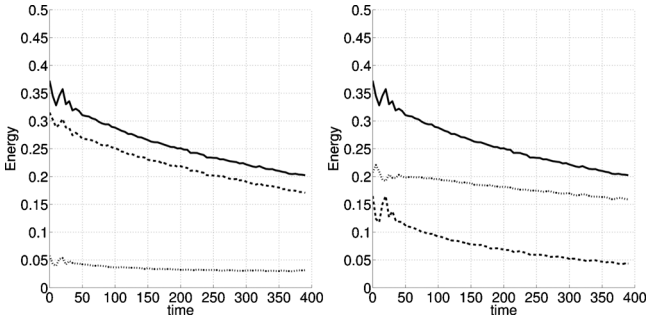

FIG. 10. Evolution of the total (solid), kinetic (dashed), and available potential (dotted) energy (left panel) of the modon, and evolution of the energy of the cyclone (dashed) and anticyclone (dotted) compared to the total (solid) energy of the modon (right panel).

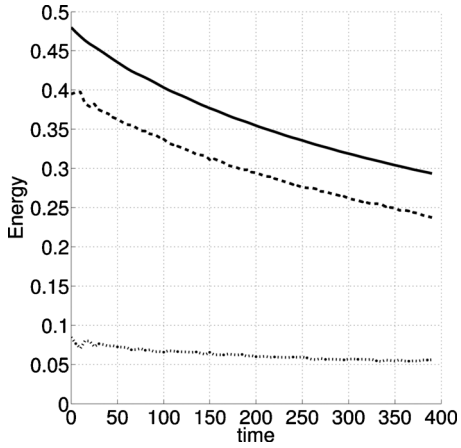

FIG. 11. Evolution of the total (solid), kinetic (dashed), and available potential (dotted) energy of the whole calculation domain.

strophic adjustment with decreasing Rossby number, propagating along trajectories with lesser and lesser curvature, and remaining closer and closer to initial geostrophic modon. For example, a QG modon with Ro=0.04 is nearly stationary (not shown). Moreover, the measure of agestrophic motions D, see Eq. (2.4), is $\mathcal{O}(\mathrm{Ro}^2)$ as compared to typical circulation in this case.

C. Adjustment of unbalanced initial configurations

We thus demonstrated the emergence of coherent ageostrophic structures as a result of adjustment of balanced dipolar initial conditions at high enough Ro. A question arises whether they will appear also as a result of the adjustment of unbalanced initial conditions. As extreme examples of such conditions, we have taken a QG modon velocity field without thickness perturbation and the QG thickness field without velocity perturbation. We present below only the simulations with initial conditions corresponding to large Ro, small-Ro initial conditions giving the QG modons as a result of the adjustment process (not shown).

1. Dipolar wind anomaly without pressure perturbation

As the initial conditions for this simulation we take the same velocity field with Ro=0.2, as in the previous one, but no thickness perturbation at all. Figures 12 and 13 give the evolution of the thickness and velocity and of the PV field, respectively, for this simulation. After the initial adjustment and emission of IGW we see again the emergence of a coherent dipole of a similar form as in the previous simulation, although detrainment of the weak PV is more pronounced. We do not present the evolution beyond $t=50$, as, due to bending of the trajectory, the vortex starts to strongly interact with its trail for later times (see Fig. 13, right panel). It should be stressed that the amount of ejected PV is much greater than in the previous simulation with balanced initial conditions.

As follows from the right panel of Fig. 12, the (almost) adjusted dipole is ageostrophic, with velocity and thickness anomaly fields close to that observed for the adjusted modon in the previous simulation. The same is true for the divergence field (not shown). The value of D at $t=50$ is 0.33. The scatter plot of Bernoulli function versus PV presented in Fig. 14 shows that we indeed have a coherent structure. The black admixture on the gray vertical line, corresponding to the exterior of the dipole, is related to the detrained weak PV, see Fig. 13, right panel.

2. Dipolar pressure anomaly without wind perturbation

The opposite to the previous case is an initial pressure (thickness) anomaly without velocity perturbation. The Rossby number for such configuration cannot be defined, but it should be remembered that in order to get the geostrophic balance, not only Ro should be small, but the Burger number should be of order unity, which implies that typical normalized deviation of the free surface should be of the order Ro (see, e.g., Ref. 3). Thus, in order to have a velocity field with substantial Ro in the present case, initial thickness perturbation should be substantial, too. It is taken to be 0.5 below.

The evolution of the thickness anomaly, velocity, and PV for such initial configuration is presented in Figs. 15 and 16, respectively. The differences with the two previous cases are striking: first of all the emerging PV dipole is quasigeostrophic, as follows from the orientation of the velocity field vectors with respect to the isobars in the right panel of Fig. 15. Second, the detrainment of weak PV is quasisymmetric and the trajectory is approximately straight. Yet the dipole adjusts to a nearly coherent structure, as follows from Fig. 17.

Thus, what we observe in the present case is rather geostrophic and not ageostrophic adjustment. Due to the asymmetry in PV of the initial state (cf. Fig. 16, left panel) and weak dissipation, the system cannot end up in a steady symmetric QG modon and continues to slowly evolve being close to geostrophic equilibrium (presumably, according to the QG dynamics). The divergence field is negligible: the value of D at $t=50$ is 0.05, which confirms its QG character, as well as its typical Rossby number which is estimated as 0.01 at $t=100$.

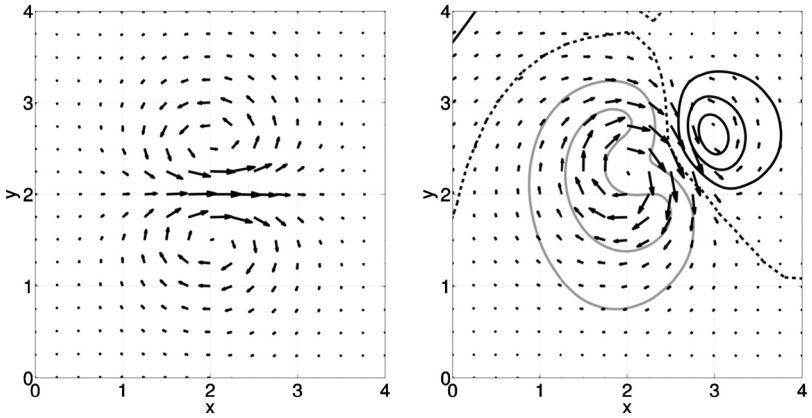

FIG. 12. Thickness and velocity field (arrows) for the adjustment of a dipolar wind anomaly at $t=0$ (left panel) and $t=50$ (right panel). Black: cyclone. Gray: anticyclone. Dotted: zero thickness anomaly line. Contour interval: 0.05. Thickness anomaly taking values in the interval $[-0.28;0.16]$ during the simulation. Only a part of the computational domain is shown.

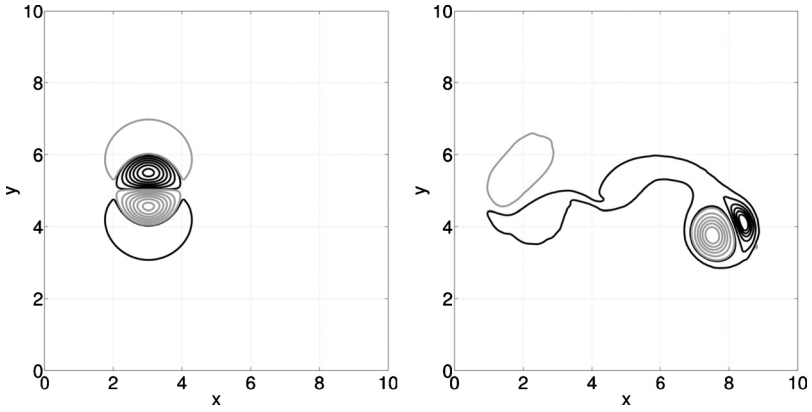

FIG. 13. Evolution of the PV anomaly for the adjustment of a dipolar wind perturbation: $t=0$ (left panel) and $t=50$ (right panel). Black: cyclone. Gray: anticyclone. Contour interval: 0.5, the lowest value of the full PV anomaly $|Q|=0.05$, PV anomaly taking values in the interval $[-3.2;3.3]$ during the simulation. Only a part of the computational domain is shown.

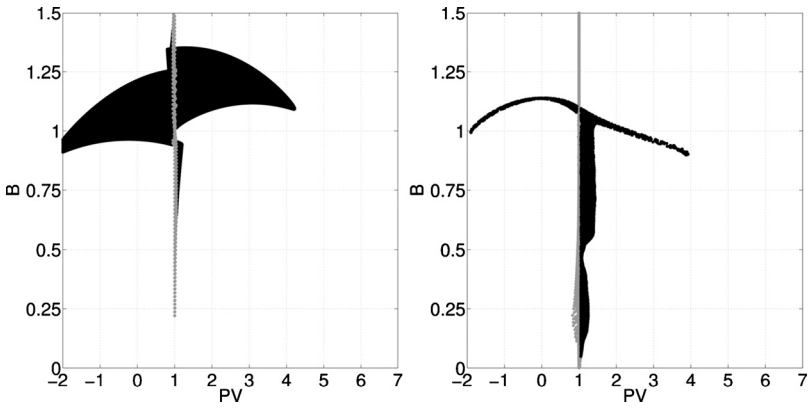

FIG. 14. Scatter plot of Bernoulli function vs PV anomaly for the adjustment of a dipolar wind anomaly at $t=0$ (left panel) and $t=50$ (right panel). Black: vortex core. Gray: outer region.

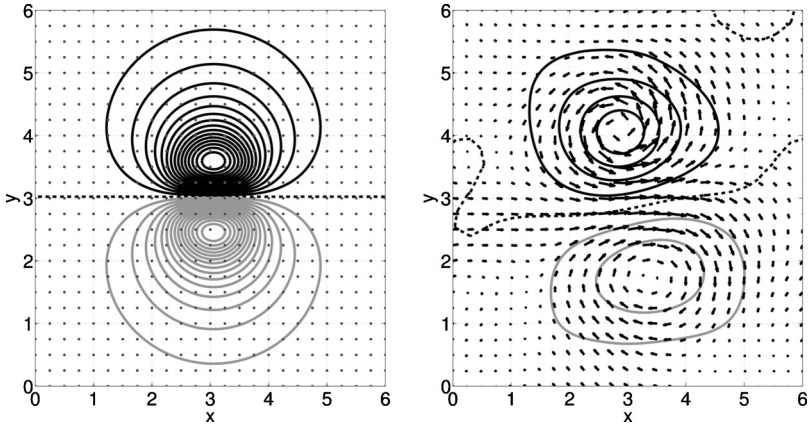

FIG. 15. Thickness (contours at the interval 0.05) and velocity field (arrows) for the adjustment of a dipolar pressure anomaly at $t=0$ (left panel) and $t=100$ (right panel). Only a part of the computational domain is shown. Black: cyclone. Gray: anticyclone. Dotted: zero thickness anomaly. Contour interval: 0.05, thickness anomaly taking values in the interval $[-0.8;0.8]$ during the simulation.

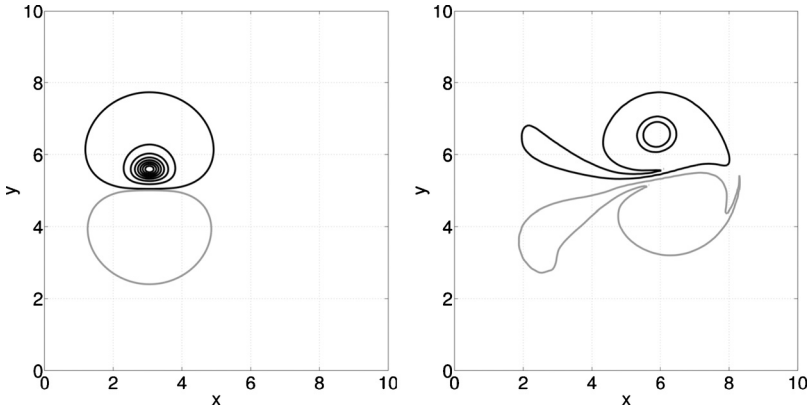

FIG. 16. PV anomaly for the adjustment of a dipolar pressure anomaly at $t=0$ (left panel) and $t=100$ (right panel). Black: cyclone. Gray: anticyclone. Contour interval: 0.5, the lowest value of the full PV anomaly $|Q|=0.05$, PV anomaly taking values in the interval $[-0.5;4.0]$ during the simulation.

D. Preliminary conclusions

Thus, the displayed simulations show that for initial conditions characterized by strong enough dipolar anomaly of PV, coherent long-living dipolar ageostrophic vortices emerge as a result of adjustment process. They are asymmetric, with dissipation acting stronger on the higher-gradient cyclonic partner, which leads to the bending of the dipole trajectory toward the anticyclonic vortex. Permanent detrainment of weak cyclonic PV accompanies the displacement of the vortex. Although the denomination ageostrophic modons was used to describe the exact solutions in Ref. 6, we will abusively call in the same way the adjusted coherent ageostrophic vortices emerging in our simulations, the difference between the two will be stressed when necessary (see Sec. IV below).

To understand the degree of universality of such scenario, it should be reminded that in the absence of dissipation the Lagrangian conservation of PV engenders an infinite series of Eulerian conservation laws of the form

$$\int dxdyH\mathcal{F}(q) = \text{const.}, \tag{2.6}$$

where the integration is over the whole domain of the flow and $\mathcal{F}$ is an arbitrary function. Thus, in the absence of dissipation the fluid motion takes place on the surfaces (leafs) of constant conservation laws. A (weak) dissipation provides a (slow) drift across such leafs. Even if exact solutions of inviscid equations exist on some of the leafs, as suggest the results of Ref. 6 to be discussed below, as well as the simulations presented above, it is unclear how wide the family of these solutions is and how solutions change from one leaf to the other, as they are not known analytically.

III. AGEOSTROPHIC MODONS AS COHERENT STRUCTURES: ILLUSTRATIONS

In this section we give a couple of illustrations of coherence and robustness of the ageostrophic modons found in the simulations presented above. For initializations we take one (or more) adjusted dipole(s) of the simulation of Sec. II B (in fact we cut off from the simulation output a portion of the computational domain containing the dipole) and use it as initial conditions.

A. Anomalous transport of a passive tracer by ageostrophic modons

The ageostrophic modon is sufficiently intense to capture fluid particles in its core and transport them along its trajectory (ballistic transport), as shown in Fig. 18, where we uniformly seeded a passive tracer, marked in gray, in a rectangle containing the modon (left panel). Subsequent evolution (right panel) shows that a part of the tracer is captured in the vortex cores and ballistically transported, and another part is detrained with a positive PV filament. Thus, ageostrophic modons, if present in the flow, will significantly influence its transport properties providing anomalous transport.

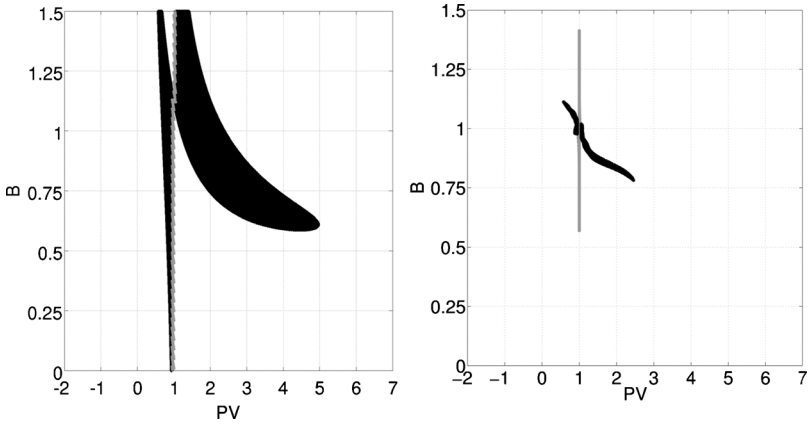

FIG. 17. Scatter plot of Bernoulli function vs PV anomaly for the adjustment of a dipolar pressure anomaly at $t=0$ (left panel) and $t=100$ (right panel). Black: vortex core. Gray: outer region.

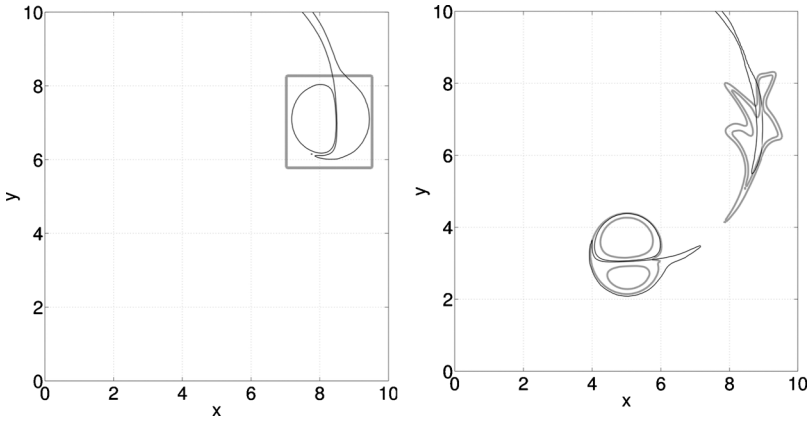

FIG. 18. Transport of a passive tracer (gray) by an ageostrophic modon. Left panel: $t=0$, tracer is uniformly seeded in a rectangle containing the vortex cores. Right panel: $t=40$, most part of the tracer is captured in the vortex cores and ballistically transported along the vortex trajectory, while some part of the tracer is detrained with the vortex filament. Two levels of concentration of the passive tracer are chosen to display the details of the transport process. The modon is represented by the $|Q|=0.05$ contours (thin lines).

B. Elastic collisions of ageostrophic modons

To test the robustness of ageostrophic modons we performed a "crash test" by organizing frontal collisions between modons. To this end, we initialize the simulation with modons moving in opposite directions with an impact parameter (the distance between the modons' axes) approximately equal to the radius of the dipole. For a range of impact parameters we got, surprisingly, an elastic collision, as shown in Figs. 19 and 20. As follows from Fig. 19, almost straight-moving modons collide, exchange cyclonic partners, and exit without losing their coherence, at an angle with respect to the initial direction of propagation. Vortex collisions with partners exchange are known in literature (see, e.g., Ref. 15). We are not aware, however, of such interaction in compressible medium subject to gravity (=sound) wave emission due to the vortex interactions. Surprisingly enough, the IGW activity during the collision is extremely weak, in spite of non-negligible divergence field associated with the vortices.

The energetics of the collision of Fig. 19 are presented in Fig. 20. It shows that the collision is elastic. An excess of energy observed at $t\approx 40$ is apparently due to the definition of the vortex boundary as a contour of $|Q|=0.05$ through which energy may be transported.

C. Interaction of the ageostrophic modon with topography

Another illustration of robustness of the ageostrophic modon is provided by its interaction with topography. The simplest (steep) topography was chosen in a form of Heaviside function of x. The initial modon position was chosen in a way that it approaches the step in the perpendicular direction, as shown in Fig. 21, lower panel. For the low step ($\Delta h/H_0=0.05$) presented in the Fig. 21, the modon crosses the topography with a deflected trajectory while maintaining its structure. The form of the trajectory can be explained in standard terms from the PV conservation and topographic compression of fluid columns and from the point-vortex analogy. The curvature of the trajectory (see Fig. 21, lower panel) depends on the asymmetry of the dipole. Such behavior is identical to that observed in the rotating fluid experiments.[16] Again, as in such experiments, there exists a critical amplitude of the step (about 0.2) beyond which the modon loses its coherence after encountering the step (not shown).

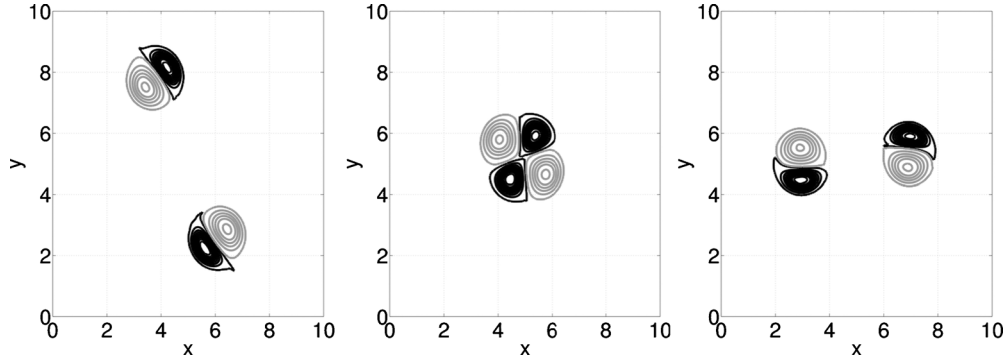

FIG. 19. PV field of frontally colliding modons at $t=25$, 40, and 50, from left to right. Black: cyclone. Gray: anticyclone. Contour interval: 0.5, the lowest value of the full PV anomaly $|Q|=0.05$. The modons exchange cyclonic partners and change the direction of propagation after the collision, without losing coherence.

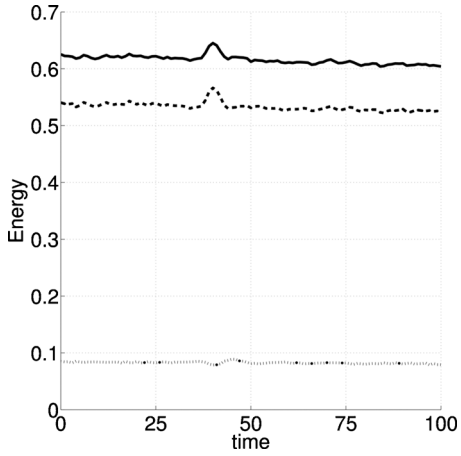

FIG. 20. Energetics of the modons' collision: total (solid), kinetic (dashed), and available potential energy (dotted) of the modons' pair as a function of time.

IV. COMPARISON BETWEEN THE AGEOSTROPHIC MODONS EMERGING FROM THE DNS, AND THE EXACT SOLUTIONS BY KIZNER *et al.*

In their pioneering paper Kizner *et al.*[6] constructed exact dipolar solutions of the full nondissipative RSW equations, which are steadily moving along the straight paths. The QG modon configurations (2.3) were used as a starting point for iterative procedure for solving the RSW equations written in the comoving frame, which combined analytical and numerical calculations. Thus, for the first time the ageostrophic modon solutions were obtained, although their analytic expression remains unknown.

It should be emphasized that this procedure does not preserve the values of the conserved quantities (2.6) of the original QG modon configuration, and thus the solution does not remain on the same leaf in the parameter space (see the discussion in Sec. II D above). It would be natural to expect that these solutions arise as a result of the adjustment process. However, as we have seen, this is not the case, at least in what concerns the bending of trajectories, relative amplitudes of cyclonic and anticyclonic components and detrainment of the cyclonic PV observed in DNS.

Yet, dissipation being presumably responsible for the latter phenomena, it is instructive to compare the structure of the ageostrophic modons observed in the numerical experiments and predicted theoretically. Inspection showed that in a series of profiles of theoretical ageostrophic modons, kindly provided by Kizner, the one obtained from the QG modon with Ro=0.12 is closest to the dipole resulting from the DNS of Sec. II B. Detailed comparison, however, reveals rather significant differences. The section of the thickness field across the centers of the vortices and corresponding sections of the PV field are presented in Fig. 22. While the

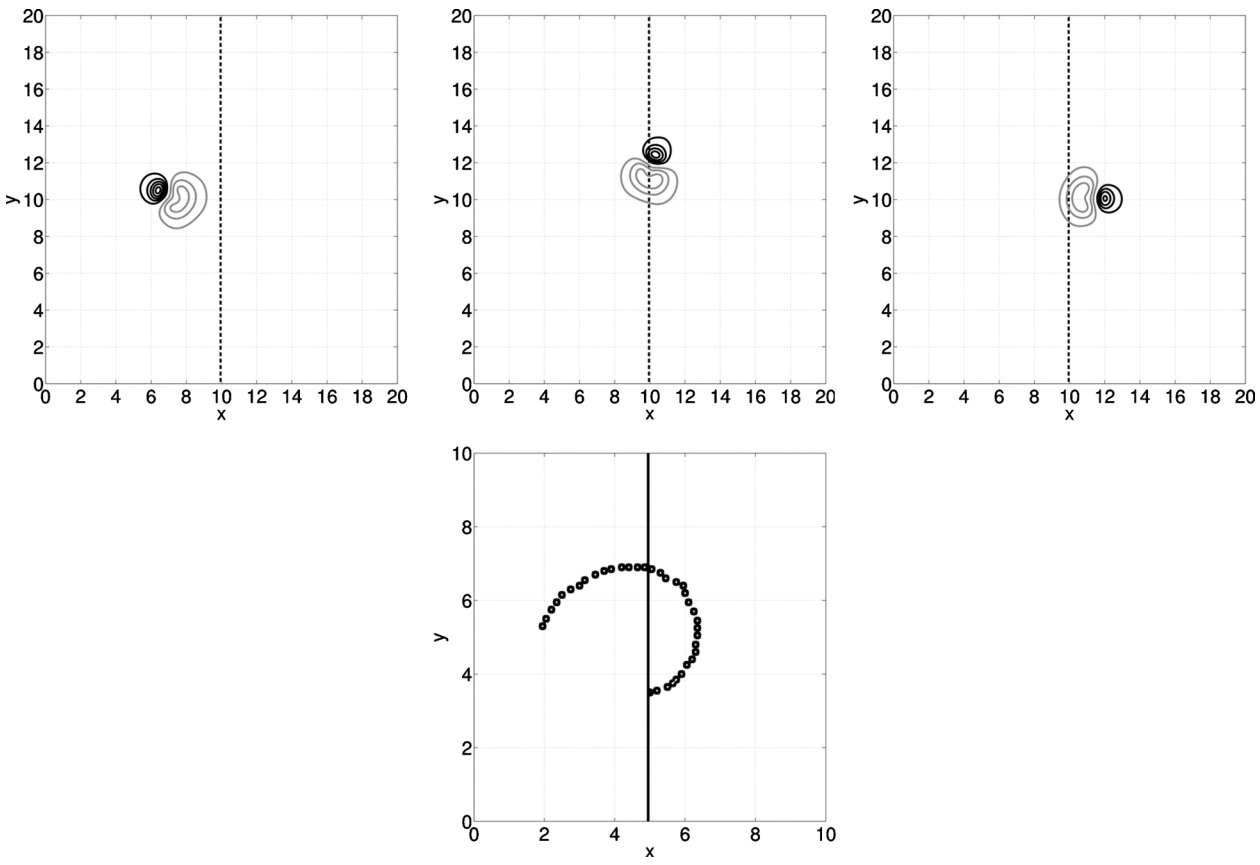

FIG. 21. Upper panels: thickness anomaly of the ageostrophic modon crossing a steplike topography from deep (left of the dashed line) to shallow (right of the dashed line) water. The relative amplitude of the step is 0.05, $t=10$, 40, and 60 from left to right, respectively. Black: cyclone. Gray: anticyclone. Contour interval: 0.05 (thickness anomaly evolving between $[-0.28;0.18]$ during the simulation). Lower panel: trajectory of the modon (the straight line marks the topography jump) points at time interval 2.

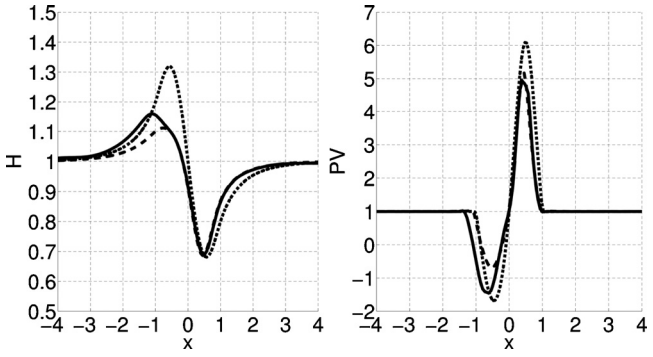

FIG. 22. Comparison of the profiles of thickness (left panel) and PV (right panel) for theoretical (dashed) ageostrophic modon obtained starting from QG modon with Ro=0.12 and the modon arising in DNS of the adjustment problem at $t=100$ (solid). Initial profiles of the QG modons are plotted in the dotted line.

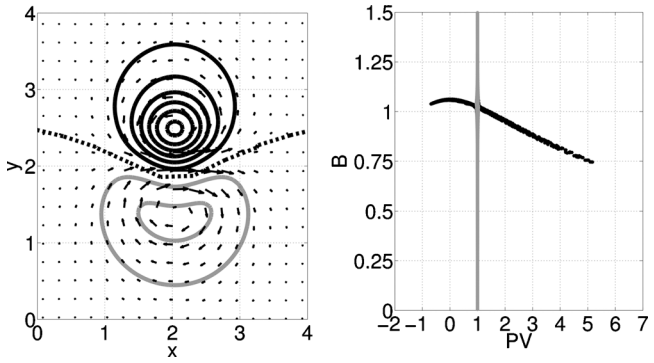

FIG. 23. Distribution of velocity and thickness (left panel) and B-PV scatter plot for the theoretical ageostrophic modon.

cyclonic parts show almost absolute coincidence, the anticyclonic parts diverge, the anticyclonic PV anomaly and elevation of the experimental modon being much higher and more spread.

The two-dimensional distributions of thickness and velocity fields are also different. There are differences in scatter plots as well, as follows from Fig. 23, to compare with Figs. 5 and 9. Again, the differences are concentrated in the anticyclonic part of the dipole, which is more spread out and less balanced (more ageostrophic) in the experimental modon, as follows from the comparison of Fig. 23, left panel, and Fig. 5, right panel. Comparison of the right panel of Fig. 23 with the right panel of Fig. 9 shows, once more, the differences in the anticyclonic (negative PV anomaly) parts of the two structures.

It is difficult to explain these differences uniquely by the action of the dissipation which, as follows from Fig. 22, does diminish the peak value of PV, but not to the extent revealed by the comparison. In order to test the theoretical predictions in DNS we initialized the simulations with a fine-resolution profile of the modon, which was obtained by Kizner *et al.* starting from the QG modon with Ro=0.2. The results of this simulation are presented in Fig. 24. The initial stage of evolution is dominated by weak anticyclonic PV detrainement and weak positive curvature of the trajectory. At later stages cyclonic detrainement dominates and the curvature of the trajectory becomes positive. Moreover, the evolution of the divergence field presented in Fig. 25 shows that theoretical modon is subject to an adjustment, with weak IGW emission seen as the divergence patterns of alternating signs, and rearrangement of the initial divergence field, which is initially more symmetric and more widespread, toward a compact quadrupolar divergence pattern centered at the cyclonic vortex, typical for experimental modons (cf. Fig. 6). The evolution of the integral divergence measure D is close to that observed in the simulation of Sec. II B, although here the initial value of D is nonzero: it is ≈ 0.7 for the modon with Ro=0.2. At $t=50$ $D\approx 0.39$, $\Gamma_+\approx 2.15$, and $\Gamma_-\approx 2.2$ for the simulation of Fig. 24.

Such adjustment toward the structure of experimental modon may result either from the discretization errors in the theoretical profile, or from the fact that another exact solution exists in the parameter space close to the theoretically found one, e.g., a solution with circular trajectory. It is an indication that the domain of attraction of theoretical modons is rather narrow, if any. It is worth noting, however, that at small Ro theoretical modons are close to the QG ones and, once used as initial conditions in DNS, are moving without change of form along the quasistraight trajectories (not shown).

V. SUMMARY AND DISCUSSION

Thus, we demonstrated that balanced dipolar PV anomalies with high enough (but not unrealistically high) Rossby numbers, typically Ro=0.2, are subject to ageostrophic adjustment, and produce robust ageostrophic quasisteady dipolar vortices, while at an order of magnitude smaller Ro they follow the classical geostrophic adjustment scenario. The observed ageostrophic dipoles (modons) are close to recently found in[6] exact solutions of rotating shallow water equations, yet significant differences in the structure of the anticyclonic part of the dipoles, and in the divergence field were detected.

The observed vortices display characteristic cyclonic PV detrainement and have trajectories bended toward the anticyclonic vorticity center. These phenomena are similar to those observed in (*a priori* nonshallow water) laboratory experiments in the rotating tank, and qualitatively reproduced in numerical simulations of 2D Navier–Stokes equation with nonlinear Ekman corrections.[10] Simulations directly initialized with ageostrophic modon solutions of Ref. 6 with high enough Ro reveal similar patterns, after a period of adjustment, which indicates that the domain of attraction of these solutions is rather narrow.

We show that ageostrophic modons are surprisingly robust and undergo quasielastic collisions. They also maintain coherence while interacting with steep topography. They produce anomalous transport, again as dipoles in nonshallow water experiments[10] and mixing. It is worth noting that the evolution of the initially balanced quasigeostrophic modon we observed provides an example of "spontaneous" imbalance, see, e.g., Ref. 17, when a balanced configuration emits IGW and changes structure. This is important for understanding the sources of inertia-gravity waves.

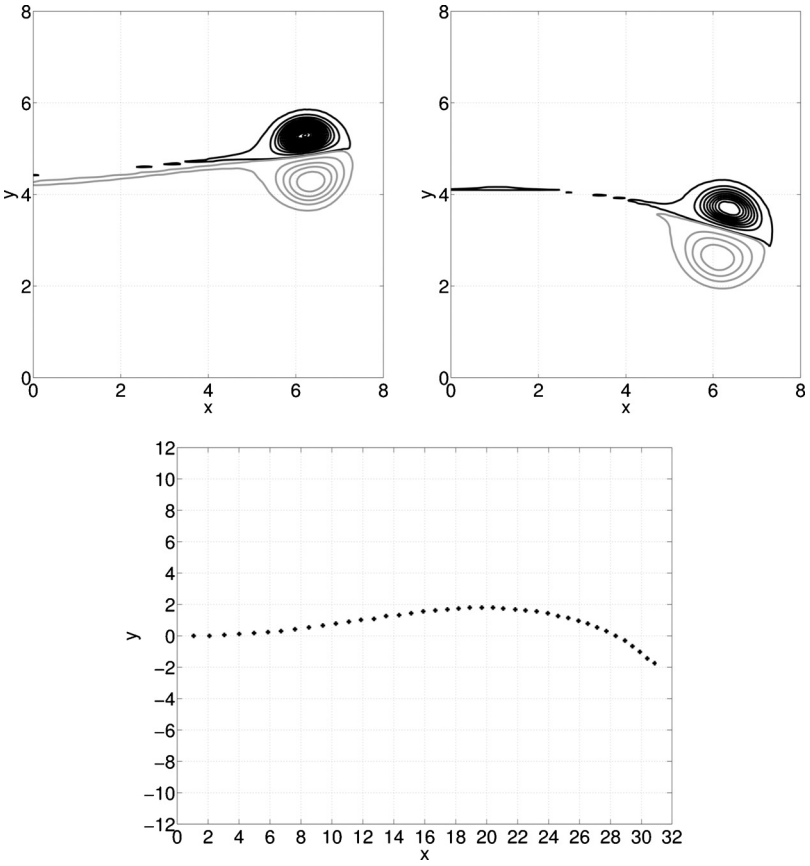

FIG. 24. Evolution of the PV field initialized by the theoretical ageostrophic modon configuration obtained from the QG modon with Ro=0.2 at $t=50$ (upper left panel) and $t=150$ (upper right panel) and the trajectory of the modon (lower panel). Black: cyclone. Gray: anticyclone. Contour interval: 0.5, the lowest value of the full PV anomaly $|Q|=0.04$, PV anomaly taking values in the interval $[-3;25]$ during the simulation.

Finally, we should mention several points which deserve further study. An important feature observed in our simulations was asymmetric evolution of the cyclone and anticyclone partners of the dipole. As gradients are higher in the cyclonic partner of the ageostrophic modon, see Fig. 22, we attributed this asymmetry mostly to the numerical dissipation. Although we have no explicit control of the dissipation in our numerical scheme, the slope limiters applied in the second-order in space version used in the simulations are a source of dissipation, which renders our hypothesis plausible. However, other explanations cannot be excluded at the present stage. Thus, as was shown in Ref. 18 by using a numerical scheme similar to ours, monopolar unbalanced anomalies of opposite sign of mass (thickness) adjust differently in RSW, the same for unbalanced momentum (velocity) anomalies: mass imbalance giving stronger cyclones and momentum imbalance giving stronger anticyclones. These conclusions were then supported by theoretical considerations using PV rearrangement technique. Although such considerations are not immediately transposable to the dipolar case, the results are consistent with what we observed in our simulations with unbalanced initial conditions. On the other hand, as was shown in Refs. 19 and 20, cyclones are less stable than anticyclones in RSW. Although we did not see obvious

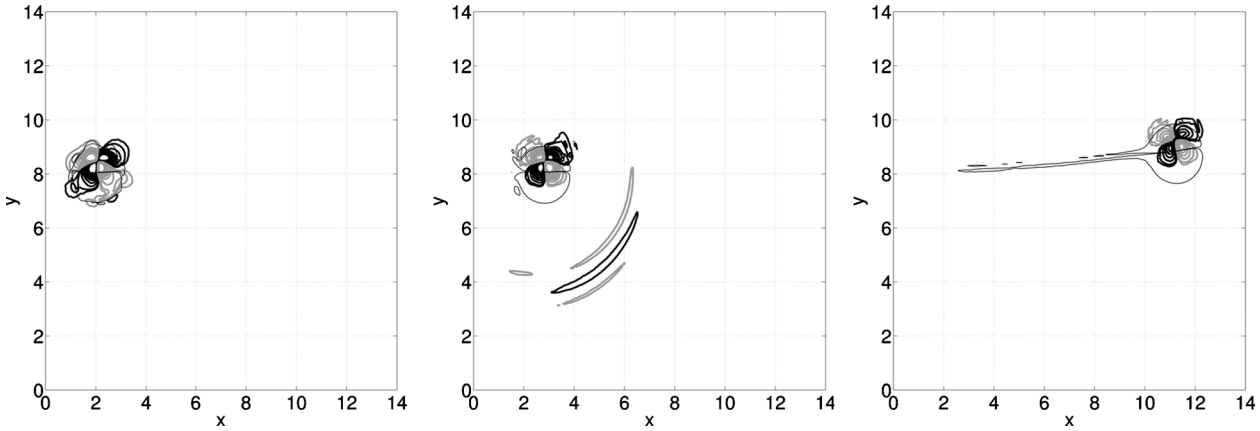

FIG. 25. Evolution of the divergence field of the initial theoretical ageostrophic modon configuration. $t=0$, 4, and 100, from left to right. Contours with small PV anomaly $|Q|=0.04$ are superimposed (thin lines) for the sake of comparison with Fig. 24. Black: divergence. Gray: convergence. Contour interval: 0.05, superimposed with a divergence field value of ± 0.03 (the divergence field taking values in the interval $[-0.8;0.9]$ during the simulation).

signs of instability developing inside the cyclonic part of the modon, we cannot exclude this mechanism (which *in fine* results in enhanced dissipation in the cyclone) without considerable increase of the resolution.

Another point is that B-PV scatter plots we used as an indicator were proved in the literature to be a line only for straight-moving solutions of the RSW equations. The fact that we observed them linelike for structures moving along a curved trajectory may mean that the observed structures are close to exact solutions moving along a circle, for which, presumably, a similar result on the relation between B and PV may be established.

ACKNOWLEDGMENTS

We are grateful to Z. Kizner for detailed and instructive discussion and for providing fine-resolution profiles of the solutions found in Ref. 6, which were used in the simulations of Sec. IV above. Stimulating discussions with G. Reznik are also gratefully acknowledged. We are grateful to him for careful reading of the manuscript and pertinent remarks which were reflected in the final version. Special thanks are to F. Bouchut for his help with the numerical code. We are also grateful to the anonymous referee for constructive comments.

[1] A. Gill, *Atmosphere-Ocean Dynamics* (Academic, London, 1982).
[2] J. Pedlosky, *Geophysical Fluid Dynamics* (Springer, New York, 1987).
[3] G. M. Reznik, V. Zeitlin, and M. BenJelloul, "Nonlinear theory of geostrophic adjustment. Part 1. Rotating shallow water model," J. Fluid Mech. **445**, 93 (2001).
[4] V. Zeitlin, G. M. Reznik, and M. BenJelloul, "Nonlinear theory of geostrophic adjustment. Part 2. Two-layer and continuously stratified primitive equations," J. Fluid Mech. **491**, 207 (2003).
[5] V. M. Kamenkovich and G. M. Reznik, *Gidrodinamika Okeana*, Fizika Okeana Vol. 2 (Nauka, Moscow, 1978), pp. 300–358.
[6] Z. Kizner, G. M. Reznik, B. Fridman, R. Khvoles, and J. McWilliams, "Shallow-water modons on the f-plane," J. Fluid Mech. **603**, 305 (2008).
[7] F. Bouchut, "Efficient numerical finite-volume schemes for shallow-water models," in *Nonlinear Dynamics of Rotating Shallow Water: Methods and Advances*, edited by V. Zeitlin (Elsevier, Amesterdam, 2007), Chap. 4.
[8] F. Bouchut, J. LeSommer, and V. Zeitlin, "Frontal geostrophic adjustment and nonlinear wave phenomena in one-dimensional rotating shallow water. Part 2. High-resolution numerical simulations," J. Fluid Mech. **514**, 35 (2004).
[9] F. Bouchut, E. Scherer, and V. Zeitlin, "Nonlinear adjustment of a front over escarpment," Phys. Fluids **20**, 016602 (2008).
[10] L. Zavala Sansón, G. J. F. van Heijst, and N. A. Backx, "Ekman decay of a dipolar vortex in a rotating fluid," Phys. Fluids **13**, 440 (2001).
[11] P. Malanotte-Rizzoli, "Planetary solitary waves in geophysical flows," Adv. Geophys. **24**, 147 (1982).
[12] V. V. Meleshko and G. J. F. van Heijst, "On Chaplygin's investigations of two-dimensional vortex structures in an invicid fluid," J. Fluid Mech. **272**, 157 (1994).
[13] Another possible choice is integrated square of divergence versus enstrophy.
[14] For this estimate, we used two parameters. One is the distance from the modon's center (defined as the equidistant point between the two maxima of PV) to the (straight) line of propagation of the geostrophic modon. The second is the ratio between the two components of the propagation speed, respectively, normal and parallel to the line of propagation of the geostrophic modon.
[15] G. J. F. van Heijst and J. B. Flor, "Dipole formation and collisions in a stratified fluid," Nature (London) **340**, 212 (1989).
[16] M. Tenreiro, L. Zavala-Sanson, and G. J. F. van Heijst, "Interaction of dipolar vortices with a step-like topography," Phys. Fluids **18**, 056603 (2006).
[17] V. Zeitlin, "Decoupling of balanced and unbalanced motions and inertia-gravity wave emission: Small versus large Rossby numbers," J. Atmos. Sci. **65**, 3528 (2008).
[18] A. C. Kuo and L. M. Polvani, "Nonlinear geostrophic adjustment, cyclone/anticyclone asymmetry, and potential vorticity rearrangement," Phys. Fluids **12**, 1087 (2000).
[19] A. Stegner and D. G. Dritschel, "A numerical investigation of the stability of isolated shallow water vortices," J. Phys. Oceanogr. **30**, 2562 (2000).
[20] J. M. Baey and X. Carton, "Vortex multipoles in two-layer rotating shallow-water flows," J. Fluid Mech. **460**, 151 (2002).